Carnegie Observatories Astrophysics Series, Vol. 3:
Clusters of Galaxies: Probes of Cosmological Structure and Galaxy Evolution, 2004
ed. J. S. Mulchaey, A. Dressler, and A. Oemler (Pasadena; Carnegie Observatories:
http://www.ociw.edu/ociw/symposia/series/symposium3/proceedings.html)

Unveiling Proto-clusters and Proto-large-scale Structures at $z > 3$ with th Subaru Prime Focus Camera

M. OUCHI[1], K. SHIMASAKU[1], H. FURUSAWA[2], S. OKAMURA[1], M. DOI[1], M. HAMABE[3], M. KIMURA[1], Y. KOMIYAMA[2], S. MIYAZAKI[2], F. NAKATA[4], M. SEKIGUCHI[1], M. YAGI[5], and N. YASUDA[5]

(1) University of Tokyo, Tokyo, Japan (2) Subaru Telescope, Hilo, USA
(3) Japan Women's University, Tokyo, Japan (4) University of Durham, Durham, UK
(5) National Astronomical Observatory, Tokyo, Japan

Abstract

We present results of our deep and wide multi-band optical surveys for clustering of galaxies at $z > 3$. We took B, V, R, i', z', and $NB711$ ($\lambda_c = 7126$Å, $\Delta\lambda = 73$Å) images in the Subaru Deep Field (SDF) and the Subaru/XMM Deep Field (SXDF), which cover a $\simeq 1200$ arcmin^2 area in total with $i' = 26.9$ and 26.2. We select 2,600 Lyman break galaxies (LBGs) and Lyman α emitters (LAEs) at $z = 3.5-5.2$. We calculate the angular correlation functions of these high-z galaxies, and find that the clustering amplitudes are strongly biased against the underlying dark matter with $b_g = 2-5$. Then we estimate the mass of dark halos hosting these high-z galaxies with the analytic model given by Sheth & Tormen. We find that the hosting dark halos have masses of $10^{10}-10^{13}M_\odot$ for LBGs at $z = 4$. We compare the number densities of the high-z galaxies with those of the total dark halos existing at $z = 4-5$. It implies that a single dark halo can host less than one LBG but more than one LAE on average. We carried out spectroscopic follow-up and additional imaging for LAEs at $z = 4.9$ in the northern field flanking the SDF. We discovered a proto-large scale structure traced by LAEs at $z = 4.9$. The structure appears a filament with a high-density core of LAEs with $r = 12$ Mpc. The core would be a proto-cluster embedded in the proto-large scale structure.

1.1 Introduction

It is essential to reveal the clustering properties of high-z galaxies for understanding the structure formation and galaxy formation in the universe. The advances of observational technology and search techniques have made possible measuring the clustering properties of high-z galaxies and to find proto-clusters at $z > 3$. Steidel et al. (1998) discovered the proto-cluster traced by the Lyman Break Galaxies (LBGs) at $z = 3.1$, and Giavalisco et al. (1998) measured the clustering amplitudes of Lyman Break Galaxies at $z = 3$. Lyman α emitter (LAE) searches around DLAs (e.g. Moller & Fynbo 2001) and radio galaxies (e.g. Venemans et al. 2002) are now popular ways to find high-density regions of high-z galaxies. We have launched surveys of two blank fields (SDF and SXDF) with the Subaru Prime Focus Camera (Suprime-Cam; Miyazaki et al. 2002), which is the optical wide-field camera mounted on 8m-Subaru. We call these surveys the Subaru Deep Surveys. In these proceedings, we present the clustering properties of LBGs and LAEs at

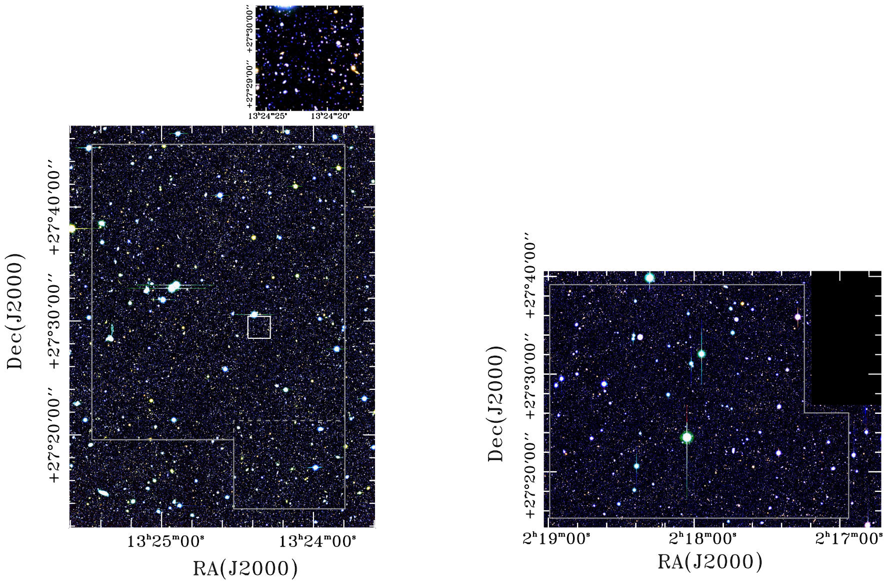

Fig. 1.1. Color composite images of the Subaru Deep Field (SDF; left) and the Subaru/XMM Deep Field (SXDF; right). The deep J, K imaging region is shown as the white box near the center of the left panel, and a magnified image of the region is shown on the upper small panel.

$z = 3.5-5.2$. We also report a proto-large scale structure at $z = 4.9$ discovered by the first follow-up observations. Throughout this paper, we use the set of the cosmological parameters: $(h, \Omega_m, \Omega_\Lambda, n, \sigma_8) = (0.7, 0.3, 0.7, 1.0, 0.9)$.

1.2 Observations and Galaxy Samples

During the commissioning runs of Suprime-Cam from November 2000 to October 2001, we carried out multi-band, deep and wide-field optical imaging with Suprime-Cam in two blank fields. One is the Subaru/XMM Deep Field (SXDF: $2^h18^m00^s$,$-5°12'00''$[J2000]) covering a 653 arcmin^2 area (right panel of Figure 1.1). The other is the Subaru Deep Field (SDF: $13^h24^m21.4^s$,$+27°29'23''$[J2000]) covering a 616 arcmin^2 area (left panel of Figure 1.1) whose central region has ultra-deep J and K' images (Maihara et al. 2001).

We took multi-color images with the B-, V-,R-, i'-, and z'-band filters for both the SDF and the SXDF, and an image with one narrow-band filter (NB711; $\lambda_c = 7126$Å, $\Delta\lambda = 73$Å) for the SDF. The total exposure time is 81 to 210 minutes for each band, and the limiting magnitudes are $i' = 26.2$ and $i' = 26.9$ for the SXDF and the SDF, respectively. During the observations, the seeing size varied from $0''.5-1''.0$ and $0''.5-0''.9$. We limit the object catalog to $i' < 26.0$ and $z' < 25.5$ for the SXDF and $i' < 26.5$ and $z' < 26.0$ for the SDF, in order to provide a reasonable level of photometric completeness. Our i'-limited and z'-limited catalogs contain respectively 39,301 (45,923) and 34,024 (37,486) objects for the SXDF (SDF).

1.2.1 Definition of BRi, Viz, and Riz-Lyman Break Galaxies

We make three photometric samples of LBGs by the following two color selections. The first sample is for BRi-LBGs at $z \sim 4$. Their Lyman break enters into the B band and thus they are identified by red $B-R$ and blue $R-i'$ colors. Similarly, the second is Viz-LBGs at $z \sim 5$ selected by $V-i'$ and $i'-z'$, and the third is Riz-LBGs at $z \sim 5$ selected by $R-i'$ and $i'-z'$. We define the selection criteria for these LBGs, so that the completeness be sufficiently high and the contamination be negligibly small. In order to determine the selection criteria for these LBGs in the two-color diagrams, we use the best-fit SEDs of galaxies given in the HDF-N photometric redshift catalog (Furusawa et al. 2000). We generate artificial galaxies that mimic the HDF-N galaxies, and distribute them randomly on our original images after adding Poisson noises according to their original brightness. Then, we detect these simulated objects and measure their brightness in the same manner as for our original images. We iterate this process 100 times, and we generate probability maps of low-z interlopers and LBGs in the two-color diagrams. Based on the probability maps, we determine the selection criteria for the LBGs which give small contaminants and keep enough completeness. The selection criteria we adopted are

$$B-R > 1.2,\ R-i' < 0.7,\ B-R > 1.6(R-i')+1.9, \tag{1.1}$$

$$V-i' > 1.2,\ i'-z' < 0.7,\ V-i' > 1.8(i'-z')+1.7, \tag{1.2}$$

$$R-i' > 1.2,\ i'-z' < 0.7,\ R-i' > 1.0(i'-z')+1.0. \tag{1.3}$$

We apply these selection criteria to our photometric catalogs, and we find 1,438 (732), 246(34), and 68 (38) objects for BRi-LBGs, Viz-LBGs, and Riz-LBGs in the SDF (SXDF) *. Table 1.1 summarizes the LBGs found in our data.

We estimate the redshift distribution, completeness (left panel of Figure 1.2) and contamination (right panel of Figure 1.2) of the LBG samples using the probability maps obtained from the simulations. The redshift distributions are $z = 4.0 \pm 0.5$ for BRi-LBGs, $z = 4.7 \pm 0.5$ for Viz-LBGs, and $z = 4.8^{+0.4}_{-0.2}$ for Riz-LBG. The ratio of real objects to contaminants in number is 1% for BRi-LBGs, 26% for Viz-LBGs, and 40% for Riz-LBGs in the SDF. The completeness of each sample is 40-60% in the most efficient redshift ranges. The small ratio of contaminants in BRi-LBGs is due to the fact that the BRi-LBG sample includes a number of faint LBGs beyond M^*, which are much more numerous than foreground contaminants.

1.2.2 Definition of Lyman α Emitters at $z = 4.9$

We make a photometric sample of Lyman α Emitters (LAEs) at $z = 4.9$ with the following criteria:

$$Ri-NB711 > 0.8, R-i' > 0.5, i'-NB711 > 0. \tag{1.4}$$

These criteria choose 87 LAEs at $z = 4.86 \pm 0.03$ with completeness $\sim 40\%$ for $NB711 < 26.0$ (details are described in Ouchi et al. 2003a).

1.2.3 Spectroscopic Follow-up Observations

Spectroscopic follow-up observations of the LBGs and LAEs started in March 2001, with the multi-object spectroscopic mode of Subaru/FOCAS (Kashikawa et al. 2002).

* The V-band image of the SXDF is not deep enough to select Viz-LBGs with a small number of contaminations. In order to avoid a large number of contaminants, we adopt $V-i' > 1.2,\ i'-z' < 0.7,\ V-i' > 1.8(i'-z')+2.3$ as the Viz-LBG selection criteria for the SXDF.

Table 1.1. *Photometric Samples of Galaxies*

Field Name	Sample Name	Detection Band	Number	Magnitude Range
SDF	BRi-LBG	i'	1,438	$i' = 23.5 - 26.5$
SDF	Viz-LBG	z'	246	$z' = 24.0 - 26.0$
SDF	Riz-LBG	z'	68	$z' = 24.0 - 26.0$
SXDF	BRi-LBG	i'	732	$i' = 23.5 - 26.0$
SXDF	Viz-LBG	z'	34[a]	$z' = 23.5 - 25.5$
SXDF	Riz-LBG	z'	38	$z' = 24.0 - 25.5$
SDF	z=4.9 LAE	$NB711$	87(43)	$NB711 = 24.0 - 26.0(25.5)$

[a]Viz-LBG of SXDF is selected by the criteria shown in the footnote.

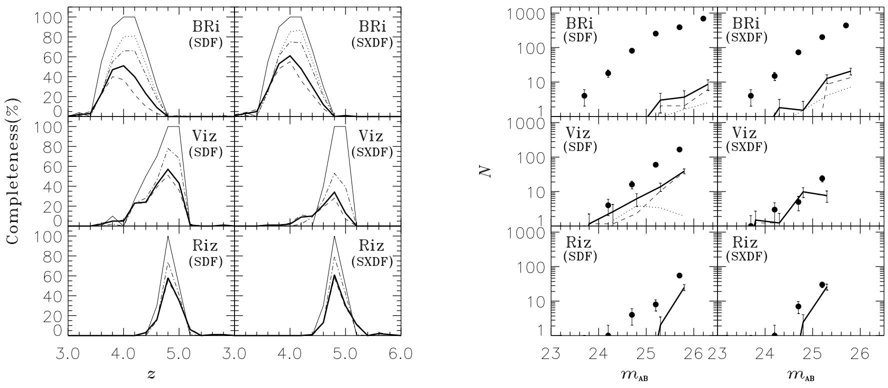

Fig. 1.2. Left panel shows the redshift-completeness diagrams of our LBG samples. Dotted, dot-dashed, and dashed lines are completeness for sources with 24.25, 25.25, 26.25 mag for BRi-LBGs and 24.75, 25.75 mag for Viz-LBGs and Riz-LBGs. Thin solid lines show the completeness when the sources have infinitely high signal-to-noise ratios. Thick solid lines are the number-weighted completeness down to the detection limits. Right panel shows numbers of contaminants as a function of magnitude. Solid (dashed and dotted) lines show total (foreground galaxies' and stars') numbers of contaminants in each magnitude bin. Filled circles are number counts of our LBG samples.

Details of the redshift distributions are shown in Kashikawa et al. (2003). These observations are now going-on. We show 5 spectra of the LAEs (Shimasaku et al. 2003) at $z = 4.9$ in Figure 1.3. The spectra, *A*-*E*, correspond to five LAEs shown by the filled circles in Figure 1.8. They have a single emission line in the wavelength range of 4700-9400Å. Thus the five objects are either an LAE or an [OII] emitter. We conclude that *A*, *B*, *D*, and *E* are LAEs at $z = 4.9$ while *E* is probably an [OII] emitter at $z = 0.9$ from the asymmetric shapes of emission lines and the continuum break measured with $V - i'$ color (Shimasaku et al. 2003). Since one out of five LAEs is a foreground interloper, the contamination of the LAE sample is thought to be $\sim 80\%$.

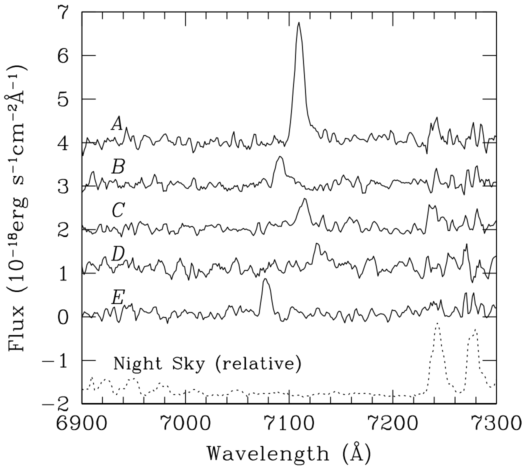

Fig. 1.3. Spectra of five LAEs over the wavelength range 6900-7300Å. Fluxes of objects *A*,*B*,*C*, and *D*, have been offset for clarity by 4×10^{-18}, 3×10^{-18}, 2×10^{-18}, and 1×10^{-18} ergs s^{-1} cm^{-2} Å^{-1}, respectively. The relative spectrum of the night sky emission is shown by a dotted line; emission lines are not present around 7100Å.

1.3 Clustering Properties of Galaxies at $z = 3.5 - 5.2$

We show the sky distribution of the LBGs and LAEs in Figure 1.4. In order to measure the clustering properties of galaxies, we derive the angular two-point correlation, $\omega(\theta)$, using the estimator defined by Landy & Szalay (1993). We find clustering signals with significant levels in the BRi-LBGs of the SDF and SXDF, and in the Viz-LBGs and the Riz-LBGs of the SDF (Figure 1.5). We fit a single power-law, $\omega(\theta) = A_\omega \theta^{-\beta}$, to the data points. Since the angular correlation functions show clustering properties of galaxies projected on the sky, the amplitudes of $\omega(\theta)$ reflect a combination of the redshift distribution of the selected galaxies and the intrinsic amplitude of clustering in the three dimensional space. We invert the observed $\omega(\theta)$ by the Limber equation (see Peebles 1980), adopting the selection functions of our sample galaxies (Figure 1.2), obtain the correlation length, r_0, in the three dimensional two-point correlation function, $\xi_g = (r/r_0)^{-\beta-1}$. The right panel of Figure 1.5 shows the estimated r_0 as a function of redshift, together with r_0 of the underlying dark matter calculated by Peacock & Dodds (1996). This figure indicates that the correlation amplitudes of LBGs and LAEs are much stronger than those of the underlying dark matter. We define the galaxy-dark matter clustering bias as $b_g = \sqrt{\xi_g/\xi_{DM}}$ at $8h_{100}^{-1}$ Mpc, where ξ_{DM}

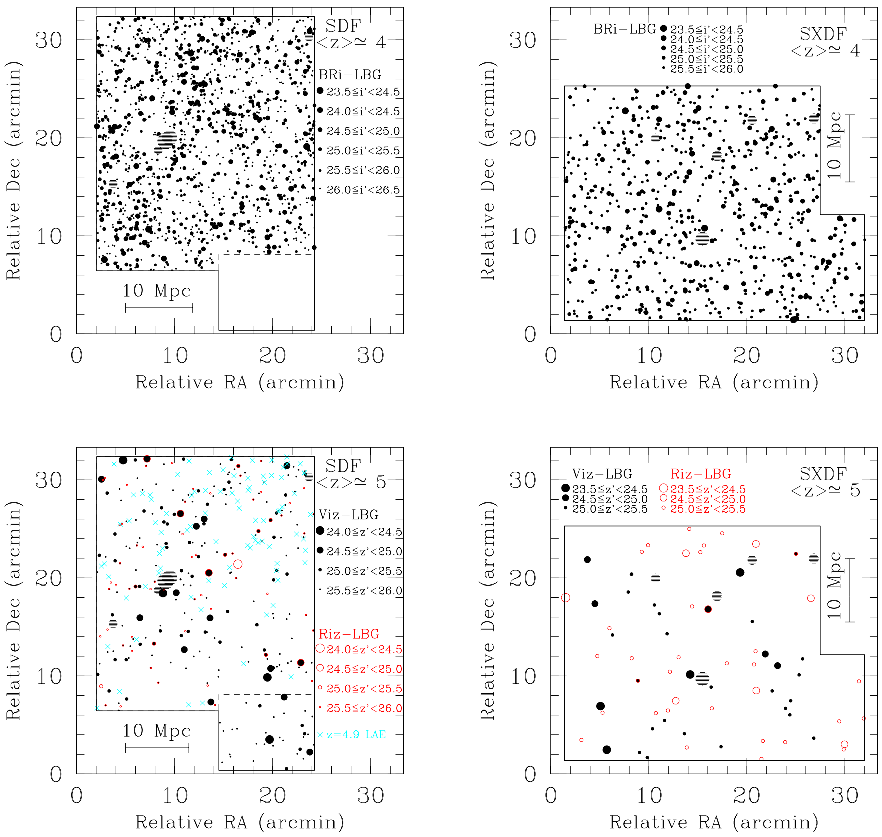

Fig. 1.4. Sky distribution of LBGs at $z = 4$ and LBGs and LAEs at $z = 5$ in the SDF and SXDF.

is the two-point correlation function of the underlying dark matter. The right panel of Figure 1.5 shows b_g vs. redshift. LBGs and LAEs are biased against dark matter by 2-5 in b_g, and the bias becomes stronger at higher redshifts. This increase in LBGs' bias can be considered as a piece of evidence of the biased-galaxy formation scenario (e.g. Baugh et al. 1999).

Since we have a large number (~ 1400) of the $z = 4$ LBGs, we examine the magnitude dependence of the clustering amplitude (r_0 and b_g) with four subsamples binned according to the source brighness ($\Delta m = 1.5$). Figure 1.6 plots the correlation length (and the bias) for the four subsamples as a function of magnitude. Figure 1.6 indicates that bright LBGs have strong clustering, which is a tendency similar to that found for present-day galaxies (Norberg et al. 2002) and LBGs at $z = 3$ (Giavalisco & Dickinson 2000). We find from this figure that brighter galaxies are more strongly clustered, although galaxies fainter than M^* have almost the same clustering amplitude. We fit the four points of m vs. b_g with a function (Norberg's law), $b/b^* = a + (1-a)L/L^*$, where we adopt L^* as the value measured for the luminosity function of $z = 4$ LBGs ($i^* = 25.3$; Ouchi et al. 2003b). We obtain $b^* = 2.8$ and $a = 0.58$, while the best-fit Norberg's law of the present-day galaxies is $a = 0.85$ (Norberg et

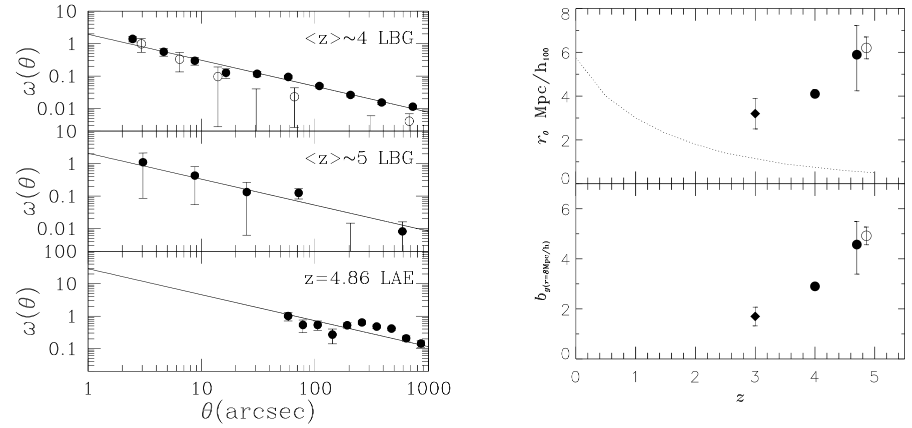

Fig. 1.5. *Left* : Angular correlation functions of LBGs and LAEs at $z = 4-5$. *Right* : Correlation length (r_0) and galaxy-dark matter bias (b_g) as a function of redshift. The filled circles indicate our LBGs at $z = 4-5$, and filled diamonds are for LBGs at $z = 3$ (Giavalisco & Dickinson 2000). These LBGs at $z = 3-5$ have a similar brightness ($\gtrsim L^*$). The open circles indicate our LAEs at $z = 4.9$. The dotted line shows the correlation length of the underlying dark matter (Peacock & Dodds 1996).

al. 2002). The coefficient, a, of $z = 4$ LBGs is smaller than that of the present-day galaxies. It may indicate that the clustering amplitudes of $z = 4$ LBGs depend strongly on the luminosity, and/or that the luminosity dependence of clusteirng is different between the rest-frame UV luminosity (for LBGs) and the optical luminosity (for the present-day galaxies).

1.4 Hosting Dark Halos

We estimate the mass of dark halos hosting the LBGs and LAEs with the analytic model given by Sheth & Tormen (1999), which is the modified Press-Schechter model fitted with the results of GIF simulation (GIF/Virgo collaboration; e.g. Kauffmann et al. 1999). Since the bias values of LBGs and LAEs are measured in $\gtrsim 1$ Mpc (physical length), measured bias reflects the bias of dark halos (which host the galaxy) vs. dark matter rather than the bias of the galaxy/galaxies (in one dark halo) vs. dark matter. We derive the mass of dark halos corresponding to the bias values obtained in section 1.3, assuming that the mass-to-luminosity ratio is constant in each bin which we measure the bias. We also calculate the number density from the luminosity functions given by Ouchi et al. (2003b) (The ticks in Figure 1.6 show the correspondences thus obtained.) We then reconstruct the mass function of dark halos hosting our galaxies at $z = 4-5$. Figure 1.7 plots the mass function derived in this way, together with the mass function of all dark halos existing at these redshifts (Sheth & Tormen 1999).

Left panel of Figure 1.7 shows that dark halos hosting LBGs are embedded in dark halos with mass of $10^{10}-10^{13}M_{\odot}$. This figure indicates that the occupation number (number per dark halo) of very bright LBGs is near unity, but that of L^* LBGs is one order smaller. This may imply that most of the low-mass ($\sim 10^{11}M_{\odot}$) dark halos do not have a galaxy. However, LBGs are star-forming galaxies which are bright in the UV. It is possible that the low-mass dark halo would have a galaxy which happens to be between star-forming phases and thus

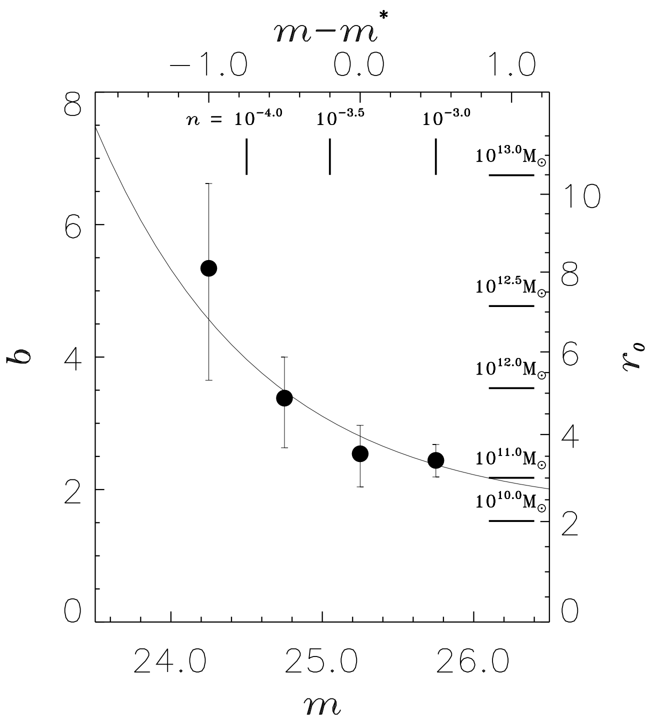

Fig. 1.6. Magnitude dependence of the correlation length, r_0, and the galaxy-dark matter bias, b_g, for LBGs at $z = 4$ in the SDF. Filled circles are the correlation lengths of the four subsamples. The solid line shows the scaled Norberg's law. Ticks in the x-axis indicate the number density of observed LBGs calculated by the luminosity function (Ouchi et al. 2003b). Ticks in the y-axis show the mass of the hosting dark halos calculated from b_g using Sheth & Tormen (1999).

escapes from our UV-selected samples (Ferguson et al. 2002). This figure implies that the dark halos hosting $z = 4$ LBGs have a minimum mass of $\simeq 10^{10} M_\odot$, if the extrapolation of the Norberg's law down to $M_{1700} = -15$ is valid.

The right panel of Figure 1.7 shows that LBGs and LAEs at $z = 5$ are embedded in dark halos with $\sim 10^{12} M_\odot$. This figure could indicate that the majority of dark halos with $\sim 10^{12} M_\odot$ do not host $z = 5$ LBGs, while hosting multiple LAEs.

1.5 Discovery of the Large-Scale Structure at $z = 4.9$

The sky distribution of LAEs in the SDF shows a large density gradient from north to south (Ouchi et al. 2003a). In order to examine how far the density gradient extends, we carried out additional imaging with $NB711$, R, and i' bands, of a northern field flanking the SDF (Shimasaku et al. 2003). Figure 1.8 shows the whole region we have imaged. We find 43 LAEs with $NB711 < 25.5$ ($> 5\sigma$) in the whole imaged region which corresponds to $100 \times 50 h_{70}^{-1}$ Mpc^2 at z=4.9 in comoving units. The LAEs are found only in a belt-like (or filamentary) region with $20 h_{70}^{-1}$ Mpc width and $> 50 h_{70}^{-1}$ Mpc length, which extends from

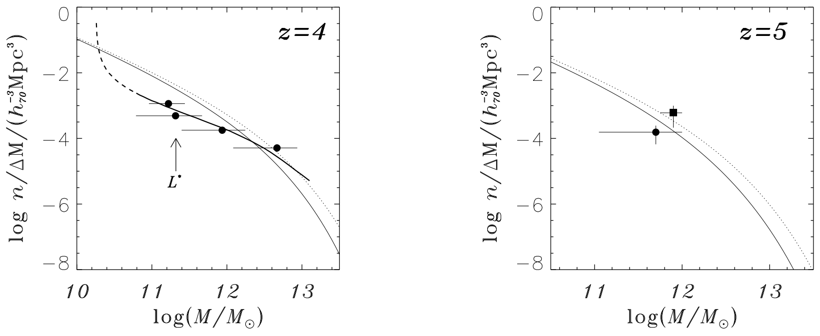

Fig. 1.7. Mass function of dark halos hosting the LBGs and LAEs at $z = 4$ (left panel) and $z = 5$ (right panel). The ΔM shown in the vertical axis means the number density in the mass range of 1 magnitude, i.e. $\Delta M = M/(2.5log(e)) = 0.92M$. Thin solid (thin dotted) line indicates the total dark halos existing at $z = 4$ predicted by Sheth & Tormen (1999) with $\sigma_8 = 0.8$ ($\sigma_8 = 0.9$). Filled circles (filled square) show mass of the LBGs (LAEs) and the number density of the LBGs (LAEs) calculated from the luminosity functions (Ouchi et al. 2003b). In left panel, the four filled circles correspond to four data points shown in Figure 1.6. Thick solid (thick dashed) line shows the result of the best-fit Noberg's law in the mass range where data exist (extrapolated down to $M_{1700} = -15$).

east-southeast to west-northwest. No previous study has revealed such a large structure, since the surveyed areas of high-z galaxies have been limited to an order of $\sim 10 \times 10h_{70}^{-1}$ Mpc^2. This is the first discovery of a large-scale structure traced by LAEs at $z = 4.9$.

Figure 1.8 shows a high-density peak (an $r = 12h_{70}^{-1}$ Mpc sphere with $\delta n/\bar{n} > 2$) of LAEs in the west part of the filamentary structure. This high-density peak may be a proto-cluster embedded in the filamentary large-scale structure, which is similar to those found in the present-day universe. We examine whether this high-density peak can be reproduced with the standard CDM model (spherical collapse model). We find that the presence of a single high-density peak in our surveyed volume is consistent with the model, if we assume that the galaxy-dark matter bias is as high as ~ 6 (Shimasaku et al. 2003). We also find in Figure 1.8 that many pair and multiple LAEs whose separations are $\lesssim 1$ Mpc. This would support the idea that LAEs are multiple galaxies hosted by one dark halo, which is implied from the large-scale angular clustering (see section 1.4). If we use the results given in section 1.4, this large-scale structures would be composed of a number of dark halos whose masses are $\sim 10^{12}M_\odot$. We will carry out follow-up spectroscopic observations for the pair and multiple LAEs at the end of March 2003 with Subaru/FOCAS, and examine the three-dimensional distribution of the LAEs in the large-scale structure.

Acknowledgments: We would like to thank the Subaru Telescope staff for their invaluable help in commissioning the Suprime-Cam that made these difficult observations possible. We thank C. Steidel and J. Ostriker for useful comments in the conference. M. Ouchi acknowl-

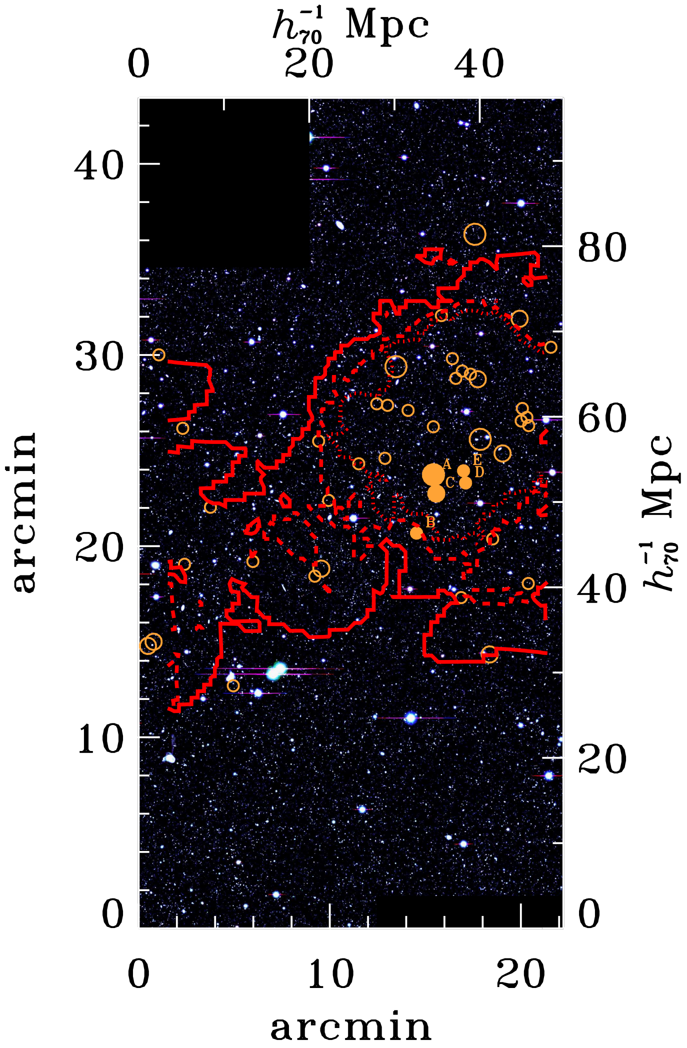

Fig. 1.8. Large-scale structure traced by LAEs at z=4.9. Circles indicate the positions of LAEs (43 in total); small, middle, and large circles denote the magnitude range of $NB711 = 24.0-24.5$, $24.5-25.0$, and $25.0-25.5$, respectively. Filled circles labeled *A*-*E* are LAEs with spectra shown in Figure 1.3. Solid, dashed, dotted contours show density contrasts of the LAEs with $\delta n/\bar{n} = 0,1,2$, respectively. North is up and east is to the left in this image.

edges support from the Japan Society for the Promotion of Science (JSPS) through JSPS Research Fellowships for Young Scientists.

References

Baugh, C. M., Benson, A. J., Cole, S., Frenk, C. S., & Lacey, C. G. 1999, MNRAS, 305, L21
Furusawa, H., Shimasaku, K., Doi, M., & Okamura, S. 2000, ApJ, 534, 624
Ferguson, H. C., Dickinson, M., & Papovich, C. 2002, ApJL, 569, L65
Giavalisco, M., Steidel, C. C., Adelberger, K. L., Dickinson, M. E., Pettini, M., & Kellogg, M. 1998, ApJ, 503, 543
Giavalisco, M. & Dickinson, M. 2001, ApJ, 550, 177
Kashikawa, N. et al. 2002, PASJ, 54, 819
Kashikawa, N. et al. 2003, AJ, 125, 53
Kauffmann G., Colberg J. M., Diaferio A., & White S. D. M., 1999, MNRAS, 308, 188
Landy, S. D. & Szalay, A. S. 1993, ApJ, 412, 64
Maihara, T. et al. 2001, PASJ, 53, 25
Miyazaki, S. et al. 2002, PASJ, 54, 833
Möller, P. & Fynbo, J. U. 2001, A&A, 372, L57
Norberg, P. et al. 2002, MNRAS, 332, 827
Ouchi, M. et al. 2001, ApJL, 558, L83
Ouchi, M. et al. 2003a, ApJ, 582, 60
Ouchi, M. et al. 2003b, in preparation
Peacock, J. A., & Dodds, S. J. 1996, MNRAS, 280, L19
Peebles, P. J. E. 1980, The Large-Scale Structure of the Universe (Princeton: Princeton Univ. Press)
Shimasaku, K. et al. 2003, ApJL, 586, L111
Sheth, R. K. & Tormen, G. 1999, MNRAS, 308, 119
Steidel, C. C., Adelberger, K. L., Dickinson, M., Giavalisco, M., Pettini, M., & Kellogg, M. 1998, ApJ, 492, 428
Venemans, B. P. et al. 2002, ApJL, 569, L11